

Journal of Biomedical Optics

BiomedicalOptics.SPIEDigitalLibrary.org

Real-time monitoring of hemodynamic changes in tumor vessels during photoimmunotherapy using optical coherence tomography

Chia-Pin Liang
Takahito Nakajima
Rira Watanabe
Kazuhide Sato
Peter L. Choyke
Yu Chen
Hisataka Kobayashi

Real-time monitoring of hemodynamic changes in tumor vessels during photoimmunotherapy using optical coherence tomography

Chia-Pin Liang,^a Takahito Nakajima,^b Rira Watanabe,^b Kazuhide Sato,^b Peter L. Choyke,^b Yu Chen,^{a,*} and Hisataka Kobayashi^{b,*}

^aUniversity of Maryland, Fischell Department of Bioengineering, 2218 Jeong H. Kim Engineering Building, College Park, Maryland 20742, United States

^bNational Institute of Health, National Cancer Institute, Molecular Imaging Program, Bldg 10, Room B3B47, Bethesda, Maryland 20892-1088, United States

Abstract. Photoimmunotherapy (PIT) is a cell-specific cancer therapy based on an armed antibody conjugate that induces rapid and highly selective cancer cell necrosis after exposure to near-infrared (NIR) light. The PIT treatment also induces the superenhanced permeability and retention effect, which allows high concentrations of nanoparticles to accumulate in the tumor bed. In our pilot studies, optical coherence tomography (OCT) reveals dramatic hemodynamic changes during PIT. We developed and applied speckle variance analysis, Doppler flow measurement, bulk motion removal, and automatic region of interest selection to quantify vessel diameter and blood velocity within tumors *in vivo*. OCT imaging reveals that blood velocity in peripheral tumor vessels quickly drops below the detection limit while the vessel lumen remains open (4 vessels from 3 animals). On the other hand, control tumor vessels (receive NIR illumination but no PIT drug) do not show the sustained blood velocity drop (5 vessels from 3 animals). Ultraslow blood velocity could result in a long drug circulation time in tumor. Increase of the blood pool volume within the central tumor (shown in histology) may be the leading cause of the periphery blood velocity drop and could also increase the drug pool volume in tumor vessels. © The Authors. Published by SPIE under a Creative Commons Attribution 3.0 Unported License. Distribution or reproduction of this work in whole or in part requires full attribution of the original publication, including its DOI. [DOI: [10.1117/1.JBO.19.9.098004](https://doi.org/10.1117/1.JBO.19.9.098004)]

Keywords: photoimmunotherapy; optical coherence tomography; Doppler optical coherence tomography; speckle variance; tumor microenvironment.

Paper 140398R received Jun. 23, 2014; revised manuscript received Aug. 11, 2014; accepted for publication Aug. 29, 2014; published online Sep. 24, 2014.

1 Introduction

Photoimmunotherapy (PIT) is a cell-specific cancer therapy with minimal side effects, which is based on an armed antibody conjugate that induces rapid cellular necrosis after exposure to near-infrared (NIR) light. The conjugate consists of a hydrophilic photosensitizer phthalocyanine dye, IR700, which is covalently bound to a humanized monoclonal antibody. When exposed to NIR light, the conjugate induces highly selective and rapid cancer cell death both *in vitro* and *in vivo*.^{1,2} It has been hypothesized that the selective destruction of the perivascular layers of cancer cells by PIT leads to expansion of the tumor vessel diameter and results in a 24-fold increase in the accumulation of various nanomaterials in the tumor bed. This effect is most marked for nanosized molecules including nanoscale anti-cancer drugs and thus reflects a relative increase in the permeability of vessels for larger molecules.³ This effect has been termed superenhanced permeability and retention (SUPR) to differentiate it from the more modest-enhanced permeability and retention that is commonly seen in tumors. Histology and fluorescence imaging with fluorescently labeled macromolecules confirms that high concentrations of non-specific nanomaterials can permeate into the tumor bed after PIT. However, little is known about the specific effects of PIT on vessel size and blood flow changes at a microscopic

level. In this study, we used intravital optical coherence tomography (OCT) to monitor the dynamics of the tumor vasculature during PIT.

OCT is an emerging biomedical imaging tool which provides depth-resolved images similar to ultrasound images.⁴ However, OCT sends light waves instead of sound waves into tissues and thus has much better spatial resolution than ultrasound (~10 μm). OCT can provide high resolution three-dimensional images of tumor microarchitecture, including the vessels and lymphatics.⁵ OCT has been widely used in cancer research to study both cellular and vascular responses to cancer therapy.⁶ For instance, Doppler OCT (DOCT) has been used to monitor vascular changes caused by photodynamic therapy.⁷ However, it remains challenging to obtain *in situ* information without resorting to window chamber-implanted tumors due to motion artifacts. In this study, we overcome this challenge with real-time motion gating using speckle variance (SV) imaging. Furthermore, we develop a vessel lumen recognition algorithm to automatically quantify the size of the lumen and measure the blood velocity. These methods can be used to monitor acute hemodynamic changes after PIT.

2 Material and Methods

2.1 Tumor Model and PIT

All *in vivo* procedures were conducted in compliance with the Guide for the Care and Use of Laboratory Animal Resources

*Address all correspondence to: Yu Chen, E-mail: yuchen@umd.edu; Hisataka Kobayashi, E-mail: kobayash@mail.nih.gov

(1996), U.S. National Research Council, and approved by the local Animal Care and Use Committee. Six- to eight-week-old female homozygous athymic nude mice were purchased from Charles River (NCI-Frederick, Frederick, Maryland). Two-million A431 cells were subcutaneously injected in the right dorsum of each of the mice. Tumors reaching $\sim 100 \text{ mm}^3$ in volume were selected for study. The conjugate of panitumumab (antiEGFR antibody) and IR700 was synthesized as previously reported.² Briefly, panitumumab (Pan, 1 mg, 6.8 nmol; Amgen, Thousand Oaks, California) was incubated with IR700 (IRDye 700DX NHS ester; $60.2 \mu\text{g}$, 30.8 nmol, 5 mmol/L in DMSO; LI-COR Bioscience, Lincoln, Nebraska) in 0.1 mol/L Na_2HPO_4 (pH 8.5) at room temperature for 60 min. The mixture (Pan-IR700) was purified with a Sephadex G50 column (PD-10; GE Healthcare, Piscataway, New Jersey). The protein concentration was determined with a Coomassie Plus protein assay kit (Thermo Fisher Scientific Inc., Rockford, Illinois) by measuring the absorption at 595 nm with spectroscopy (8453 Value System; Agilent Technologies, Santa Clara, California). The concentration of IR700 was measured by absorption with spectroscopy and the number of IR700 molecules per panitumumab was adjusted to ~ 4 . One hundred micrograms of Pan-IR700 was intravenously injected via the tail vein of a mouse 24 h before PIT. The A431 tumor was treated with continuous NIR irradiation by a 690-nm laser system (BWF5-690-8-600-0.37; B&W TEK INC., Newark, Delaware) at a power density of 167 mW/cm^2 for 10 min (100 J/cm^2). As controls, tumors in tumor bearing mice were irradiated by NIR without Pan-IR700 administration.

2.2 OCT Imaging System

One unique feature of OCT compared with conventional optical imaging modalities is its capability to resolve the information from different depths by using an interferometer. The interference fringe from different depths reveals the scattering intensity from the specific depth and has a characteristic oscillation frequency. By resolving signals with specific frequencies, a depth-resolved OCT image can be obtained. Figure 1 shows the schematic of the swept-source OCT (SS-OCT) setup. The SS-OCT system⁸⁻¹⁰ utilizes a wavelength-swept laser as its light source. The spectrum bandwidth of the laser is 100 nm centered at 1325 nm (Thorlabs, Newton, New Jersey, SL1325-P16), which gives a $10\text{-}\mu\text{m}$ axial resolution in tissue. The wavelength-swept frequency is 16 kHz with a 12-mW output power; therefore, for 1000 axial line images, the frame rate is equivalent to 16 frames/s (8 frames/s if only one direction is used). A Mach-Zehnder interferometer receives 3% of the laser output power and uses it to generate a clock signal with a uniformly spaced optical frequency to trigger the sampling of the OCT signal in the analog-to-digital converter. The circulator sends the photons from port 1 to port 2 and the reflected light from port 2 to port 3. The sample and reference arms of a Michelson interferometer receive equal portions of the remaining 97% of the laser power. The galvanometer scanning mirrors deflect the sample arm light into the sample through an objective lens, which provides a $15\text{-}\mu\text{m}$ lateral resolution. The backscattering light from the tissue is recombined with the reflected light from the reference mirror, and the interference fringe is detected by the dual-balanced detector. The signal will be acquired by the data acquisition card and then be sent to the computer for image construction and display.

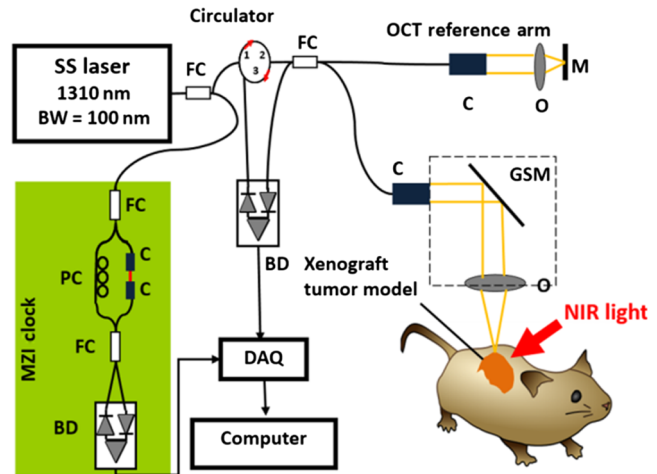


Fig. 1 Schematic of the swept-source optical coherence tomography (OCT) system. SS laser: swept source laser. FC: fiber coupler. PC: polarization controller. BD: balanced detector. C: collimator. O: objective lens. GSM: galvo scanning mirrors. M: mirror.

2.3 Phantom Studies

Figures 2(a) and 2(b) show the results of the phantom study. Two imaging protocols, DOCT¹¹ and SV,¹² are tested with a vessel phantom. The vessel phantom is a capillary tube with a 0.4-mm-inner diameter. Intralipid solution (1% volume concentration) was pushed through the tube at various speeds controlled by an injection pump (Fisher Scientific, Rockingham County, New Hampshire, Single Syringe Pump). Figure 2(a) shows that SV can accurately map the lumen of vessel, but DOCT reaches a detection limit at low velocities. SV is capable of mapping out the vessel lumen even when the bulk flow speed is zero. On the other hand, Fig. 2(b) shows that DOCT linearly changes with the flow velocity, but SV does not vary with the flow velocity. Therefore, we utilize DOCT to measure the flow velocity and SV to measure vessel diameter. The standard deviation is calculated from 10 different images under a specific flow velocity.

2.4 Bulk Motion and ROI

During the *in vivo* experiment, tissue bulk motion can significantly degrade the image quality. For example, in Fig. 2(c), when the tissue is moving (frames 263 and 264), the SV contrast between the tissue and vessel is poor. When the tissue is at rest (frames 259 and 266), the signal from the static tissue is reduced and the vessel is detectable. In Fig. 2(c), we plot the total SV signal against the frame index. Since SV is decoupled with the blood velocity and only relates to the motion of scatters, the local maximum is not related to the pulsation but only reflects that the tissue is moving. Therefore, by searching the local minimum (marked by red triangles), we can easily distinguish images with good vessel/tissue contrast from those disturbed by bulk motion and eliminate those frames with motion degradation. The DOCT images from frames with bulk motion are also removed from analysis.

In order to accurately measure the vessel lumen, we implemented an algorithm which isolates the vessel signal from the background noise. Figures 2(d)–2(g) demonstrate the procedure using representative images. In the first step, we convert the image to a binary image [Fig. 2(e)]. In the second step, we used a MATLAB (MathWorks Inc., Natick, Massachusetts) built-in

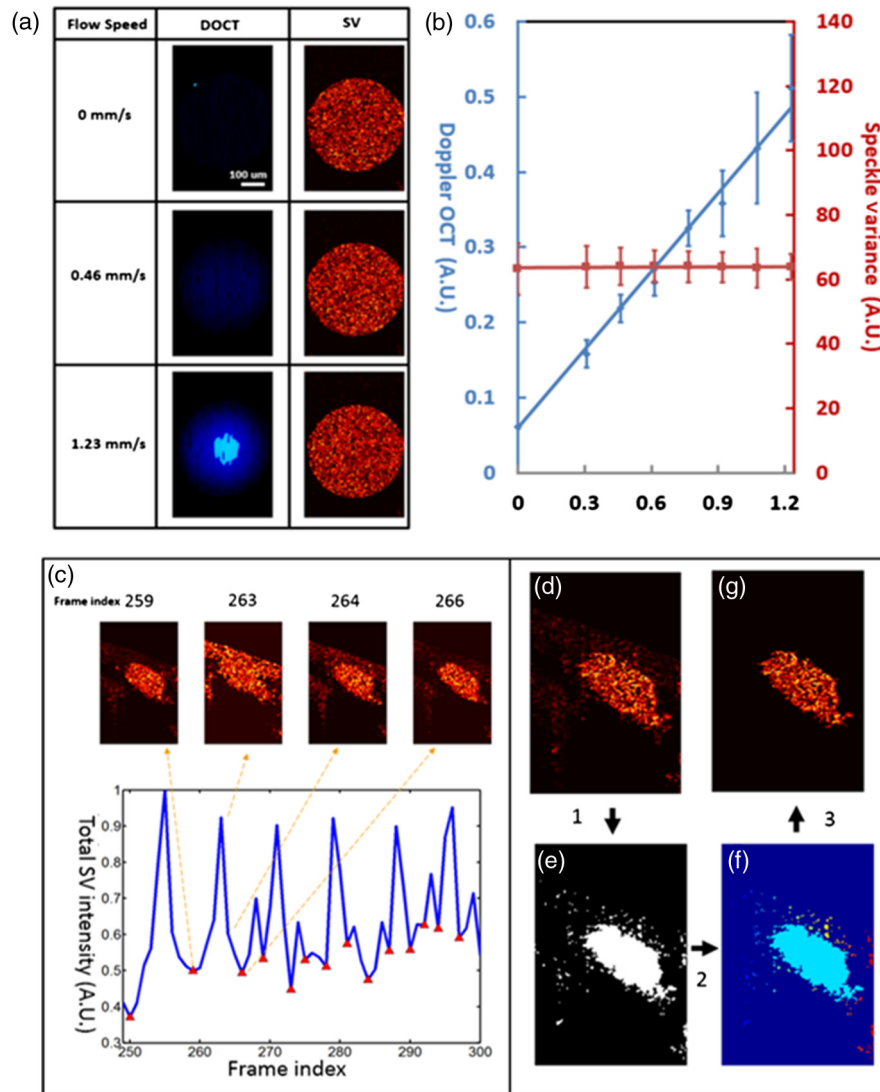


Fig. 2 (a) Cross-sectional Doppler OCT (DOCT) and speckle variance (SV) images of a vessel phantom (0.4-mm-inner diameter) at various flow velocity. (b) Total intensity of DOCT and SV versus flow velocity. (c) Real-time motion detection using SV images (6 frames/s). Frames 259 and 266 show the SV images when the tissue is at rest. Frames 263 and 264 show the SV images when the tissue is moving. By locating the local minimum (indicated by the red triangles), we can isolate images with no motion. (d to g) Automatic region of interest (ROI) selection procedure. (d) The original image with blood vessel and background noise. (e) Binary conversion of (d). (f) An image with all the connected pixels labeled with a specific color. Noise is dramatically reduced when choosing the ROI with the largest area. (g) The final image without the background noise.

function to label the connected components [Fig. 2(f)]. Figure 2(f) shows that the connected pixels are then labeled in one color. The color with the largest area is selected as the region of interest (ROI). In the final step, we overlay this ROI with the original image to isolate the vessel signal from the background [Fig. 2(g)]. Since OCT cannot penetrate the entire diameter of large vessels, we cannot use the area of the cross section to represent the size. Thus, the length of the blood vessel along each row is determined and the median measurement is chosen to represent the vessel size.

2.5 Statistical Analysis

Data are expressed as mean \pm standard deviation. Statistical analyses were carried out using MATLAB. Student *t* test was

used to compare vessel size and flow speed of treated tumors to the untreated control. $P < 0.05$ was considered to indicate a statistically significant difference.

2.6 Histopathologic Evaluation

Excised tumors underwent histopathologic examination after formalin fixation and paraffin embedding. All samples were then serially sectioned at 40- μ m intervals and stained with hematoxylin-eosin (H&E) or platelet/endothelial cell adhesion molecule-1 (PECAM-1/CD31, an vascular endothelial maker) immunohistochemical staining using an anti-CD31 rabbit polyclonal antibody (Abcam, Cambridge, Massachusetts) and a goat anti-rabbit IgG (HRP) (Abcam) as the first and second antibodies, respectively.

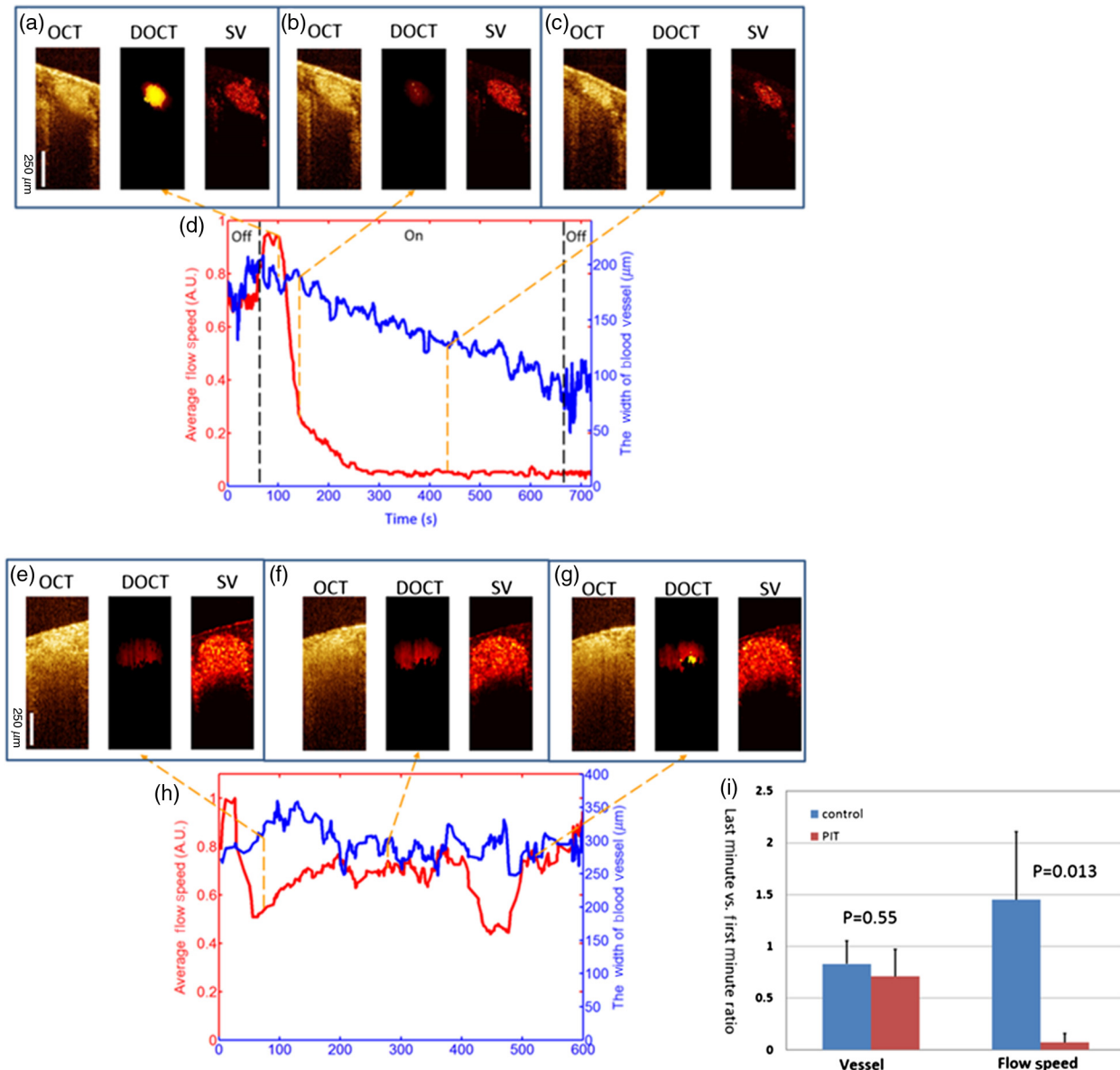


Fig. 3 Vascular changes in a photoimmunotherapy (PIT)-treated and a control tumor blood vessel. (a to c) Representative OCT/DOCT/SV images at different time points (indicated by the orange dashed lines) during the PIT treatment. (d) Time plot of the blood velocity (red line) and the vessel width (blue line). In the first 60 s (indicated by the black dashed line), the laser light is off to obtain baseline information. After 60 s, near-infrared (NIR) laser light is turned on for 10 min (60 to 660 s). The dosage is 100 J/cm². In the last 60 s (660 to 720 s), the light is turned off to obtain post-treatment information (indicated by the second black dashed line on the right). (e to g) Representative OCT/DOCT/SV images at different time points (indicated by the orange dashed lines) of a control tumor blood vessel (with NIR light, but no PIT drug). (h) Time plot of the blood velocity (red line) and the blood vessel width (blue line) of the control vessel. The dosage is 100 J/cm². (i) Ratio of vessel size and blood velocity in PIT-treated and control tumors (control is NIR irradiation but no PIT drug). The vessel size of PIT-treated vessels ($n = 4$, from 3 mice) is slightly smaller than its size in the first minute, but it is not statistically significant ($P > 0.05$) compared to the control ($n = 5$, 3 mice). On the other hand, the blood velocity of PIT-treated blood vessels drops significantly in the end of treatment compared to the beginning and it is statistically different from the control ($P < 0.05$).

3 Results

Figures 3(a)–3(d) show the diameter and the blood velocity of a PIT-treated tumor blood vessel. OCT provides the structure information. DOCT provides the blood velocity information and SV provides the size of the open lumen. The first 60 s are obtained as a baseline before PIT. At 60 s, NIR irradiation (100 J/cm²) is turned on and the blood velocity quickly drops below the detection limit. The open space in the vessel lumen also decreases with

time, but remains open after 600 s of light irradiation. After 600 s, the NIR light is turned off and post-treatment data is obtained for another 60 s. The vessel size and the velocity remain at a relatively constant level after irradiation. At the beginning of irradiation, the DOCT image [Fig. 3(a)] demonstrates that blood velocity is high and the SV image shows a large lumen. After 83 s of irradiation, the DOCT image [Fig. 3(b)] shows that the velocity has significantly decreased, but the size of the lumen remains almost unchanged. The

blood velocity drops below the detection limit after 372 s of irradiation, but the lumen remains open [Fig. 3(c)].

Control experiments were performed on mice that did not receive the antibody-photosensitizer conjugate but underwent light exposure. Figures 3(e)–3(h) show that blood velocity and lumen size during the 600 s of NIR irradiation fluctuate moderately, which is probably due to physiologic variation and motion, but there is no sustained blood velocity drop in the controls. Indeed, the images show that the blood velocity and the lumen size remain essentially the same throughout the measurement period.

To quantify the effect of PIT, the ratio of the blood velocity and lumen size at the beginning and end of PIT (comparing the first and last minute during irradiation) was determined [Fig. 3(i)]. The PIT-treated group consisted of 4 tumor vessels from 3 different animals. Control experiments (with irradiation but no drug) were performed on 5 tumor vessels from 3 different animals. The lumen size of PIT-treated tumor vessels decreased with time (the ratio is smaller than 1), but it is not statistically different from the control vessels (T test, $P > 0.05$). On the other hand, the drop in blood velocity in PIT-treated blood vessels was statistically different compared with the control group ($P < 0.05$). We conclude that while there are small nonsignificant changes in vessel lumen diameter, there is a measurable acute decrease (more than one order of magnitude) in blood velocity in the PIT-treated vessels.

Figures 4(a) and 4(b) demonstrate the histology of the peripheral tumor blood vessels. With H&E staining, the red blood cells do not display a nucleus and can be found in the well-preserved blood vessels (indicated by the red arrows). The vessels in both the control and PIT-treated tumors have well-defined boundaries and are easily identifiable indicating that the vessels are not destroyed by PIT. This data is consistent with the *in vivo* result, which suggests blood vessels are not damaged. On the other hand, PECAM-1 staining [Figs. 4(c) and 4(d)], which labels the endothelial cells of blood vessels

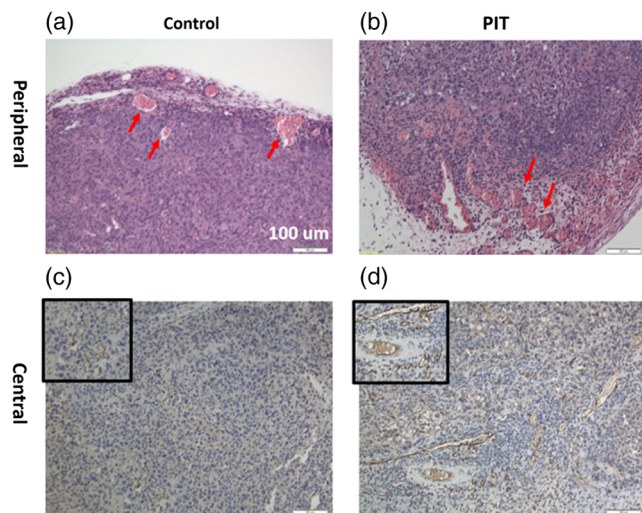


Fig. 4 (a) Histology (H&E staining) of control peripheral tumor vessel. Intact blood vessels are indicated by the red arrows. (b) Histology (H&E staining) of PIT-treated peripheral tumor vessel. Intact blood vessels are indicated by the red arrows. (c) Histology (PECAM-1 staining) of control central tumor vessel. The inset shows a zoom-in image. (d) Histology (PECAM-1 staining) of PIT-treated central tumor vessel. The inset shows a zoom-in image. The scale bar represents 100 μm .

(brown color), demonstrates that the PIT-treated capillaries in the deep tumor bed are markedly dilated compared with the control vessels.

4 Discussion

There are several advantages of using OCT in this setting. It allows us to monitor tumor vascular responses without the injection of a contrast agent or the implementation of an artificial tumor window chamber. Motion gating with SV successfully overcomes the challenge of bulk motion artifact and permits *in situ* imaging without interfering with the tumor. This method requires a fast imaging speed to obtain images not degraded by bulk motion from a breath cycle. Since the normal mouse respiratory rate is around 3 breaths per second, according to the Nyquist sampling theory, imaging speeds >6 frames/s are necessary to record the entire cycle. A high imaging frame rate limits the number of A-lines per image (more A-lines per image, slower frame rate) and thus limits the field-of-view (FOV). We used 1000 A-lines per image within a 715- μm FOV to achieve a reasonable DOCT sensitivity. The FOV could be increased by two orders to 71.5 mm while maintaining the same frame rate by using a laser source with a two orders faster wavelength sweep rate.¹³ In addition, high speed lasers can potentially enable four-dimensional tissue images. In addition to FOV, the spatial resolution could be further improved. Micro-OCT¹⁴ with a resolution of 1 μm in three dimensions will enable the detection of small vessel dilation *in vivo*.

A potential alternative will be the use of fluorescent proteins, which are excellent endogenous fluorescence emitters to be used for depicting various biological processes and cells both *in vitro* and *in vivo*. By labeling circulating cells with fluorescent proteins, blood flow in blood vessels can be clearly monitored.^{15,16} Moreover, by inserting a needle-type objective into tissue, the tumor-host interaction and their responses to the drugs can be observed *in situ*.¹⁷ These techniques are powerful tools for the development of anti-tumor drugs, but the use of fluorescence proteins requires virus-mediated *in vivo* gene transfection, which is unlikely to be permitted in humans, at least in the near future. For the practical medical application, OCT does not require any contrast agent and has been FDA approved to image retina blood flow in ophthalmic patients.¹⁸ Moreover, for either fluorescence imaging or OCT imaging, bulk motion can blur and degrade the image. In this study, we develop an algorithm that can reduce the motion artifact and permit us to image a moving tissue (see Sec. 2.4).

Unlike most other ablative therapies, both *in vivo* SV imaging [Figs. 3(a)–3(c)] and histology images [Fig. 4(b)] verify that the peripheral tumor blood vessels remain intact during PIT treatment. Furthermore, SV confirms that the vessels are filled with free moving blood cells and are not thrombosed. An obstructed vessel would result in the absence of free moving scatters and the vessel would lose its variance contrast relative to static tissue, none of which was observed. The vessels are open and filled with free moving blood cells. However, the central and peripheral vessels respond very differently. Due to the limitation of spatial resolution and penetration depth, only big ($>100 \mu\text{m}$) peripheral tumor vessels are observed *in vivo* with OCT. These big peripheral vessels do not dilate [Fig. 3(i)], while the deep capillaries are markedly dilated [Fig. 4(d)]. This heterogeneous response may be due to the difference in vessel structure. The thick peripheral vessels typically have full structures

including muscular bundles in the wall, which make them less likely to change during PIT.

Figures 3(a)–3(d) demonstrate that the blood velocity in peripheral tumor blood vessels drops significantly during PIT treatment, while the lumens of the vessels remain open. Blood velocity is maintained in control animals who received the conjugate but no light irradiation [Fig. 3(d), 0 to 60 s] and the controls who received light irradiation but no conjugate [Fig. 3(h)]. This blood velocity drop may be due to the increase of blood pool volume as a consequence of dilated central vessels. A much larger central blood pool volume as well as possible decreased intravascular pressure in the peripheral vessels could slow the blood to the periphery that could induce enhanced nanodrug delivery and reasonably explain the hemodynamic basis of the PIT-induced SUPR effect.

In conclusion, PIT treatment acutely reduces blood speed while the blood vessel is undamaged or thrombosed. Slow blood flow speed implies a long drug circulation time. On the other hand, dilated central vessels may lead to slow periphery flow and an increase in drug pool volume in tumor vessels.

In our next project, we will use multiphoton microscopy to observe the diffusion of the antibody-IR700 conjugate and estimate cancer cell viability *in situ*. This study will help elucidate how PIT destroys the perivascular barrier and enhances the delivery of anticancer drugs.

Acknowledgments

We thank UMD-NCI Partnership for Cancer Technology for supporting this study.

References

- M. Mitsunaga et al., "Near-infrared theranostic photoimmunotherapy (PIT): repeated exposure of light enhances the effect of immunoconjugate," *Bioconjug. Chem.* **23**(3), 604–609 (2012).
- M. Mitsunaga et al., "Cancer cell-selective in vivo near infrared photoimmunotherapy targeting specific membrane molecules," *Nat. Med.* **17**(12), 1685–1691 (2011).
- K. Sano et al., "Markedly enhanced permeability and retention effects induced by photo-immunotherapy of tumors," *ACS Nano* **7**(1), 717–724 (2013).
- D. Huang et al., "Optical coherence tomography," *Science* **254**(5035), 1178–1181 (1991).
- B. J. Vakoc et al., "Cancer imaging by optical coherence tomography: preclinical progress and clinical potential," *Nat. Rev. Cancer* **12**(5), 363–368 (2012).
- B. J. Vakoc et al., "Three-dimensional microscopy of the tumor microenvironment in vivo using optical frequency domain imaging," *Nat. Med.* **15**(10), 1219–1223 (2009).
- B. A. Standish et al., "Interstitial Doppler optical coherence tomography as a local tumor necrosis predictor in photodynamic therapy of prostatic carcinoma: an in vivo study," *Cancer Res.* **68**(23), 9987–9995 (2008).
- Q. Li et al., "Automated quantification of microstructural dimensions of the human kidney using optical coherence tomography (OCT)," *Opt. Express* **17**(18), 16000–16016 (2009).
- S. A. Yuan et al., "Three-dimensional coregistered optical coherence tomography and line-scanning fluorescence laminar optical tomography," *Opt. Lett.* **34**(11), 1615–1617 (2009).
- S. A. Yuan et al., "Co-registered optical coherence tomography and fluorescence molecular imaging for simultaneous morphological and molecular imaging," *Phys. Med. Biol.* **55**(1), 191–206 (2010).
- V. Yang et al., "High speed, wide velocity dynamic range Doppler optical coherence tomography (Part I): System design, signal processing, and performance," *Opt. Express* **11**(7), 794–809 (2003).
- A. Mariampillai et al., "Speckle variance detection of microvasculature using swept-source optical coherence tomography," *Opt. Lett.* **33**(13), 1530–1532 (2008).
- W. Wieser et al., "Multi-megahertz OCT: High quality 3D imaging at 20 million A-scans and 4.5 G Voxels per second," *Opt. Express* **18**(14), 14685–14704 (2010).
- L. Liu et al., "Imaging the subcellular structure of human coronary atherosclerosis using micro-optical coherence tomography," *Nat. Med.* **17**(8), 1010–1014 (2011).
- K. Yamauchi et al., "Development of real-time subcellular dynamic multicolor imaging of cancer-cell trafficking in live mice with a variable-magnification whole-mouse imaging system," *Cancer Res.* **66**(8), 4208–4214 (2006).
- K. Yamauchi et al., "Real-time in vivo dual-color imaging of intracapillary cancer cell and nucleus deformation and migration," *Cancer Res.* **65**(10), 4246–4252 (2005).
- M. Yang, P. Jiang, and R. M. Hoffman, "Whole-body subcellular multicolor imaging of tumor-host interaction and drug response in real time," *Cancer Res.* **67**(11), 5195–5200 (2007).
- Y. M. Wang et al., "In vivo total retinal blood flow measurement by Fourier domain Doppler optical coherence tomography," *J. Biomed. Opt.* **12**(4), 041215 (2007).

Chia-Pin Liang is currently a postdoctoral research fellow in Massachusetts General Hospital/Harvard Medical School, and was a postgraduate course student of the NCI-UMD joint program. He is awarded PhD (bioengineering) from the University of Maryland, College Park. His interest is in developing novel biomedical imaging tools for clinical use and basic research.

Takahito Nakajima is a visiting fellow in the molecular imaging program at the NCI/NIH in Bethesda, and an associate professor at the Gunma Graduate School of Medicine in Japan. He is awarded MD and PhD degrees (radiology and nuclear medicine) from Gunma University. His interests are in molecular imaging, novel target specific therapeutic methods, and clinical imaging in the field of radiology.

Rira Watanabe is a research scholar in the molecular imaging program at the NCI/NIH in Bethesda, Maryland. She graduated from the Hokkaido University in Japan and earned a PhD in veterinary medicine. She works in a pharmaceutical company as a senior researcher and is currently on sabbatical in the molecular imaging program as a special volunteer. Her interest is in developing therapeutic methods through novel imaging techniques.

Kazuhide Sato is a visiting fellow in the molecular imaging program at the NCI/NIH in Bethesda, and supported with JSPS Research Fellowship for Japanese Biomedical and Behavioral Researchers at NIH. He is awarded MD and PhD degree (cell pharmacology, molecular cell biology/medical science) from the Nagoya University in Japan. His interest is in developing novel therapeutic methods in oncology and pulmonology.

Peter L. Choyke is the chief of the molecular imaging program at the CCR/NCI/NIH in Bethesda, Maryland. He is a graduate of Jefferson Medical School. He joined the Diagnostic Radiology Department at the Clinical Center of the NIH in 1988 and formed the molecular imaging program at NCI in 2004. His interest is in accelerating the treatment of cancer by using novel molecular imaging agents which target specific features of cancers.

Yu Chen is an associate professor in the Fischell Department of Bioengineering at the University of Maryland College Park. He received his PhD degree from the University of Pennsylvania. He has published 60 peer-reviewed journal articles and delivered more than 50 invited talks. His research is focused on technology development of multi-modal optical imaging methods, translational device development, and biomedical applications in early cancer detection, functional neuronal/renal imaging, and tissue engineering.

Hisataka Kobayashi is the chief scientist in the molecular imaging program at the NCI/NIH in Bethesda, Maryland. He is awarded MD and PhD degrees (immunology/medicine) from Kyoto University in Japan. His interest is in developing novel molecular imaging agents and technologies, especially for targeting cancers. He has published over 250 peer-reviewed articles and 40 invited reviews and book chapters covering various modalities from basic chemistry to clinical studies.